Fs-Laser Fabrication of Photonic Structures in Glass: the Role of Glass Composition

D. M. Krol[1, 2], J. W. Chan[2], T. R. Huser[2], S. H. Risbud[3] and J. S. Hayden[4]

[1]Department of Applied Science, University of California, Davis, CA 95616, USA
E-mail: dmkrol@ucdavis.edu
[2]Lawrence Livermore National Laboratory, 7000 East Ave, Livermore, CA 94550, USA
[3]Department of Chemical Engineering and Materials Science, UC Davis, Davis, CA 95616, USA
[4]Schott Glass Technologies, Inc., 400 York Ave., Duryea, PA 18642, USA

ABSTRACT

The use of fs lasers to directly write photonic structures *inside* a glass has great potential as a fabrication method for three-dimensional all-optical integrated components. The ability to use this technique with different glass compositions- specifically tailored for a specific photonics application- is critical to its successful exploitation. Consequently, it is important to understand how glass composition effects waveguide fabrication with fs laser pulses and how different glasses are structurally modified after exposure to fs laser pulses.
We have used confocal laser spectroscopy to monitor the changes in glass structure that are associated with waveguide fabrication. Using a low power continuous wave (cw) Ar laser as excitation source we have measured both Raman and fluorescence spectra of the modified regions. Raman spectroscopy provides us with information on the network structure, whereas fluorescence measurements reveal the presence of optically active point defects in the glass.
In this paper we review our work on fs-laser fabrication and characterization of photonic structures in glass and discuss the effect of glass composition on processing parameters and structural modification.

Keywords: femtosecond laser processing, waveguides, laser spectroscopy, glass, integrated optics

1. INTRODUCTION

Femtosecond (fs) laser pulses can be used to directly "write" photonic structures, such as waveguides, splitters, interferometers etc, *inside* a glass [see for example refs. 1-9]. This technique has great potential as a fabrication technique for three-dimensional all-optical integrated components with applications in telecommunications as well as in biological and chemical sensors and medical technology. The fs writing technique relies on the fact that fs laser pulses- tightly focused inside a bulk glass- can induce localized refractive index changes of the glass within the focal volume of the laser beam. By scanning the glass with respect to the laser focus waveguide structures can be fabricated inside the glass. To fully exploit the usefulness of this technique it is important to integrate different functions into one optical component. This will require the use of different glass compositions, optimized for the optical function(s) that one wants to implement. For example, optical amplification will require a glass with high concentrations of rare-earth ions, such as a phosphate glass, whereas for optical switching a glass with a high nonlinear coefficient is needed. It is, therefore, important to understand how glass composition effects waveguide fabrication with fs laser pulses.
In order to achieve this goal the relationship between the waveguide writing parameters (pulse energies, scan speeds), waveguide properties (magnitude and spatial profile of index change, modal properties), and the glass composition needs to be investigated. In addition it is necessary to understand how the atomic-scale structure of the glass is modified after exposure to the fs laser. We have recently used a confocal microscopy/spectroscopy set-up to monitor the changes that occur in glass after exposure to femtosecond near-infrared laser pulses [8, 10-14]. Using a low power cw Ar laser as excitation source we can measure both Raman and fluorescence spectra of the modified region. Raman spectroscopy provides us with information on the network structure, whereas fluorescence measurements reveal the presence of optically active point defects in the glass.

Fifth International Symposium on Laser Precision Microfabrication, Edited by I. Miyamoto, H. Helvajian, K. Itoh, K. F. Kobayashi, A. Ostendorf, K. Sugioka, Proc. of SPIE Vol. 5662 (SPIE, Bellingham, WA, 2004) · 0277-786X/04/$15 · doi: 10.1117/12.595762

In this paper we review our work on fs laser writing in fused silica and IOG-1 phosphate glass (commercial glass from Schott Glass Technologies, Inc). We show that these two glass systems behave very differently and discuss the processes responsible for the laser-induced modification.

2. EXPERIMENTAL PROCEDURES

2. 1. Experimental setup and procedure for waveguide fabrication

We performed our experiments on polished samples of type III fused silica (Corning 7940) and IOG-1, a phosphate glass from Schott Technologies, Inc. with a nominal composition of 60% P_2O_5, 24% Na_2O, 13% Al_2O_3, 3% La_2O_3.
The experimental setup for waveguide fabrication is described in detail in ref 13. The fs laser system consisted of a Ti: sapphire oscillator (Millennia-Tsunami from Spectra Physics) and a regenerative amplifier (Merlin-Spitfire from Spectra Physics) which emitted 800 nm, 130 fs pulses at a 1 kHz repetition rate. The fs laser beam was directed through a 10x (NA = 0.25) objective using a pellicle beam splitter and focused into polished glass cubes placed on a long-travel motorized translation stage with automated motion along the z-direction. The samples were scanned along the beam axis one pass at a rate of 20 μm/s. The total scan length (and total waveguide length) of ~ 5 mm was limited by the working distance of the 10x objective. After the waveguides were written, a He-Ne cw laser at 633 nm was coupled into the waveguide through the same 10x objective. An extra long working distance (ELWD) 20x (NA=0.40) objective was used to image the near field profile of the coupled light onto a CCD camera connected to a computer. White light images of the front and back planes of the waveguide were captured using two objectives and two CCD cameras.

2. 1. Experimental setup and procedure for confocal fluorescence and Raman spectroscopy

The confocal microscopy setup used to perform spectroscopy on the modified samples is shown in Fig. 1. To acquire spectra, the glass is first exposed to fs pulses of various energies. A 50x objective is used to focus fs pulses ranging from 0.1 to 6 μJ inside the polished sample. Using a knife-edge technique, the diameter of the laser spot at the focal point is measured to be 2 μm. The laser beam is focused ~700 μm inside the glass sample, which is placed on the xyz stage. For spectroscopy of the glass a large, 3-D modified structure is first created inside the glass by scanning the sample with respect to the focused fs beam. The relatively large region is created to ensure that the Ar+ excitation beam would only probe the modified glass, thereby circumventing any issues concerning how well the 488 nm beam overlaps the fs beam, particularly in the direction of the beam propagation (z-direction in Figure 1). The region consists of three 100 x 100 μm^2 planes spaced 2 μm apart in the vertical direction (z). Each plane is made by scanning 128 100-μm-long lines spaced 0.8 μm apart at a rate of 40 μm/s. We have checked that the spectra observed for these large regions are reproduced when a spectrum of a single line is measured.

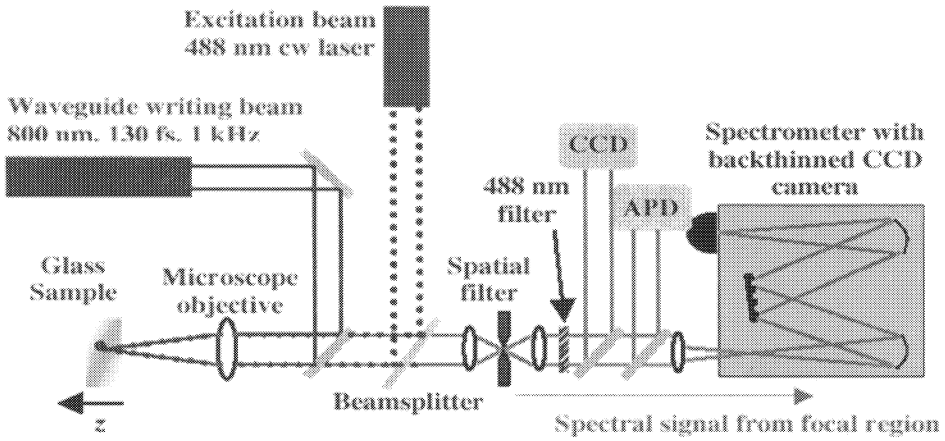

Fig.1 Scanning confocal microscope used to obtain spectroscopic signals from fs-modified glass. Flip mirrors direct fs beam through objective to modify glass. 488 nm argon ion beam probes the modified glass and spectral signals are delivered through a pinhole to a CCD camera, an avalanche photodiode detector (APD), or a spectrometer equipped with a CCD camera.

3. RESULTS

3.1 Waveguide fabrication and characterization

Fig. 2-A shows typical transmission white light images of the end face of a 5 mm long line written in fused silica and IOG-1. In the case of fused silica (fig. 2-A1) waveguiding takes place in the central region where the writing beam was focused, but in IOG-1 (fig. 2-A2) the central (exposed) region is dark and surrounded by bright regions that appear to guide the white light.

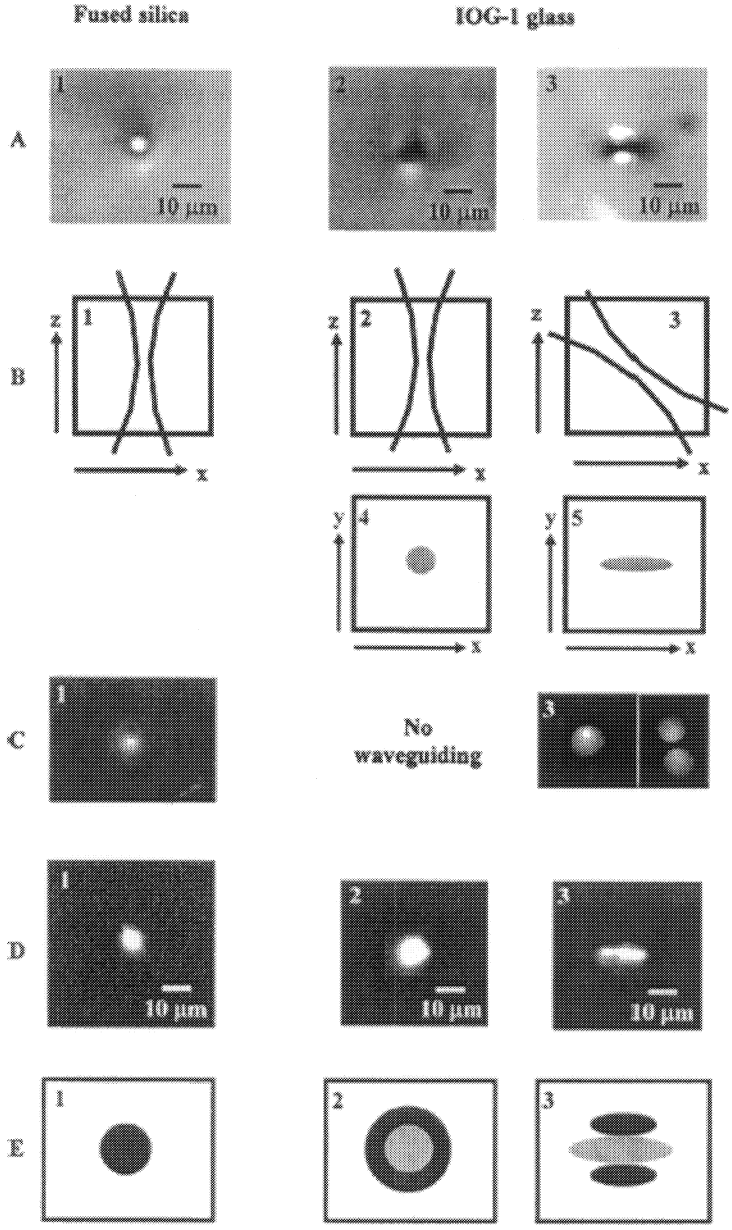

Fig. 2 Summary of waveguide writing in IOG-1 and fused silica glasses. A – White light images of the end face of laser written waveguides. B – Geometry of laser propagation direction in glass with respect to z-axis. In fig. B-III, the angle between the propagation and z-axis directions is exaggerated for clarity. C – Near field profiles at 633 nm demonstrating guiding of light in waveguides. D – Fluorescence imaging of color centers created by fs pulses. E – Refractive index profiles induced by fs pulses (dark – higher index, light – lower index). All images are shown in the x-y plane unless otherwise indicated.

We tried to further confirm this behavior by attempting to couple light from a He-Ne laser into both types of waveguides. In the case of fused silica, the He-Ne light is guided as a single Gaussian mode (fig. 2-C1) but for the IOG-1 glass no waveguiding could be observed. In further attempts to fabricate waveguides in IOG-1 glass, we slightly changed the alignment between the laser beam propagation direction and the direction along which the sample is translated during the waveguide writing process (cf figs 2-B2 and 2-B3). If the fs beam is propagated slightly off the z-axis in the xz plane while the glass is scanned along the z-axis, as shown in fig 2-B3, the behavior is significantly different. Fig. 2-A3 shows the transmission white light image of the exposed region, which is elongated in the x-direction. The dimensions are roughly 13 μm by 5 μm. Also, two "waveguide" regions, which appear elliptical in shape, appear above and below the central, dark region. These two waveguide regions have different dimensions (11 μm x 7 μm) than the central dark region. The fact that the profiles are elliptical rather than circular is caused by the slight difference between the laser beam propagation direction and the scan direction (z-axis) which results in an elliptical spot in the plane perpendicular to the scan direction (cf figs.2-B4 and 2-B5). We have carefully checked that the observed ellipticity is due to the alignment of the writing beam rather than its polarization. Rotating the polarization of the writing beam by 90° has no effect on the observed laser-induced modification. Furthermore, when the fs laser is propagated slightly off the z-axis in the yz plane, the observed microscope image is rotated 90° (i.e. a central dark region which is elliptical with the long axis along y and two waveguide regions to the left and right of the dark region). Visual changes in the glass are first visible with ~0.7 μJ fs energy, but the white light regions surrounding the dark region become noticeably visible when 1 μJ fs energy is used.
For the lines written using the geometry shown in fig. 2-B3, waveguide behavior is observed using a He-Ne laser beam. Near field profiles of 633 nm light are shown in figs. 2-C3 for the two guiding regions. Depending on the coupling conditions, light can be coupled into either waveguide or both simultaneously because of their close proximity to each other. A minimum fs energy of ~ 2 μJ is required to fabricate waveguides which guide the 633 nm light. To estimate the refractive index change associated with the waveguides, we measure the numerical aperture of the waveguides by analyzing the dimensions of the cone of light exiting the waveguide. The refractive index change is related to the numerical aperture by the equation $NA = \sqrt{2n_o\Delta n}$ for an assumed step index profile. Δn can be approximated to be roughly 1.4 x 10^{-4}. In addition, the intensity of the coupled light exiting the waveguide core is strongly dependent on the polarization of the incoming 633 nm light. A half wave plate is used to rotate the 633 nm polarization while a CCD camera is used to observe the near field profile. The coupling efficiency of the light decreases as the polarization is rotated from horizontal (E-field along major axis of ellipse) to vertical, thus confirming the elliptical nature of the waveguide shape.

3.2 Confocal Fluorescence Microscopy

The photoluminescence (PL) spectra for fused silica modified by different fs pulse energies are shown in Figure 3. 488 nm (2.54 eV) light from an argon ion laser is used as the excitation source.

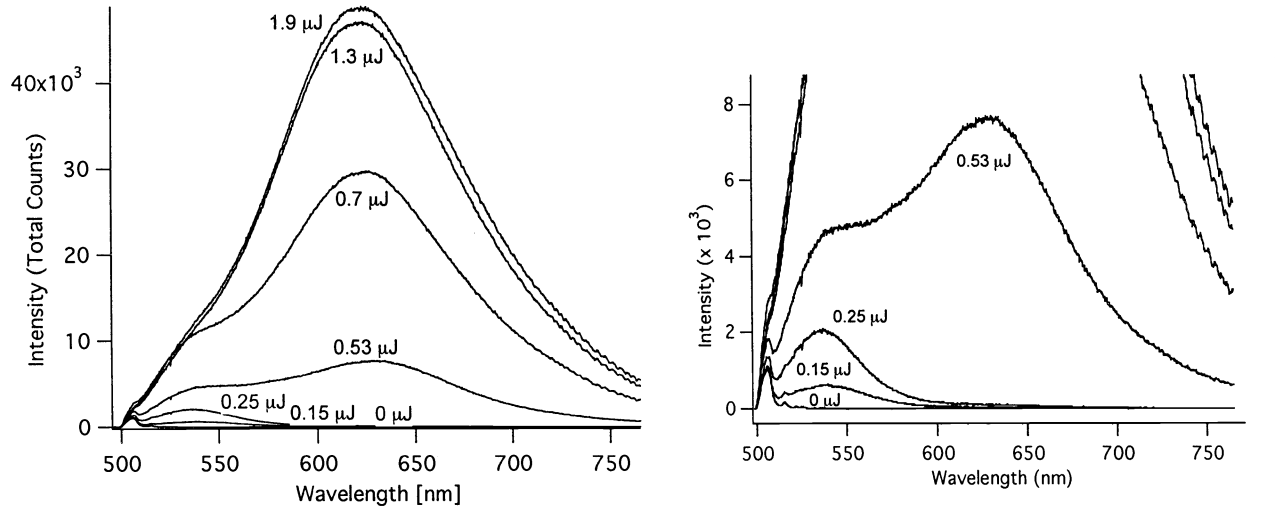

Fig. 3. PL spectra of fs-modified glass with 488 nm light as the excitation source. The set of spectra on the right show that for low fs pulse energies the 630 nm peak is not present; only a PL signal at 537 nm is observed.

At the far left (at ~ 500 nm region), weak Raman scattering signals are observed that are due to the vibrations of the silica glass network. These signals will be discussed further below. The spectra also show a broad fluorescence peak centered at ~ 630 nm (1.97 eV) that increases in intensity with increasing fs pulse energy used to modify the silica glass. The full-width-half-maximum (FWHM) is roughly 0.4 eV. It should be noted that for fs pulse energies lower than 0.25 μJ, the 630 nm peak is not appreciably observed. Figure 3b shows more detailed spectra for these low fs pulse energies. A PL peak at roughly 537 nm (2.3 eV) is clearly visible for low fs pulse energies and sits on the shoulder of the broader 630 nm peak in the higher fs pulse energy spectra. It is difficult to accurately determine the FWHM for this peak because the 630 nm peak is directly to the right and the Raman signals are directly to the left of this peak. We estimate the FWHM to be roughly 0.2 eV for the 0.25 μJ spectrum since that spectrum gives the most well-defined 537 nm signal.

A comparison of our spectral data with the optical signatures of various defects found in fused silica [15-20] indicates that defects are created in fused silica by fs laser pulses. The band centered at roughly 1.97 eV is attributed to the formation of NBOHC defects in the glass. This band is only observable at high fs laser fluences, when rough damage lines are induced in the material. At low fluences, the 630 nm band is not observable. This behavior is consistent with results obtained by Watanabe *et al.* [21] who have only observed the 1.9 eV band in silica glass modified by high fs laser intensities. At low fluences, we only observe a band at 537 nm (2.3 eV), which is assigned to the radiative recombination of (V_o; $(O_2)_i$) defect pairs. It should be pointed out that the absorption band of NBOHC defects is at 258 nm (4.8 eV). Therefore, our use of 488 nm (2.5 eV) light to excite the NBOHC defects leads us to believe that multiphoton absorption of the excitation light may be occurring.

The same procedure described above is performed to obtain fluorescence signals from modified IOG-1 glass. Figure 4 shows the PL spectra for IOG-1 phosphate glass modified with 0.3 μJ fs pulse energy using a 50x objective along with the initial spectrum of unmodified IOG-1. The initial spectrum for unmodified IOG-1 glass (with 488 nm excitation light) shows only Raman signals in the 500 – 525 nm range due to the phosphate glass network and no fluorescence bands. After modifying the glass with fs pulses, a fluorescence band centered at roughly 600 nm is observed along with the Raman signals. The peaks at roughly 590, 615, and 640 nm are artifacts of the transmission profile of a 488 nm dichroic filter used in the confocal microscope setup. It should be pointed out that the same fluorescence is observed for fs laser modified lanthanum phosphate glasses (80% P_2O_5 – 20% La_2O_3) that we have synthesized ourselves.

The fact that we observe similar fluorescence behavior in both modified IOG-1 phosphate glass and our synthesized lanthanum phosphate glasses leads us to believe that the defect centers that are created are, indeed, phosphorus related. We propose that the tightly focused femtosecond pulses create POHC color center defects that absorb the 488 nm (2.5 eV) excitation light and fluoresce at a longer wavelength of ~600 nm (2.1 eV). Our assignment is supported by a comparison of the similarities in the atomic arrangements between the POHC defect and the equivalent non-bridging oxygen hole centers (NBHOC) in fused silica. Both involve a trapped hole on an oxygen atom(s) covalently bonded to a phosphorus/silicon atom.

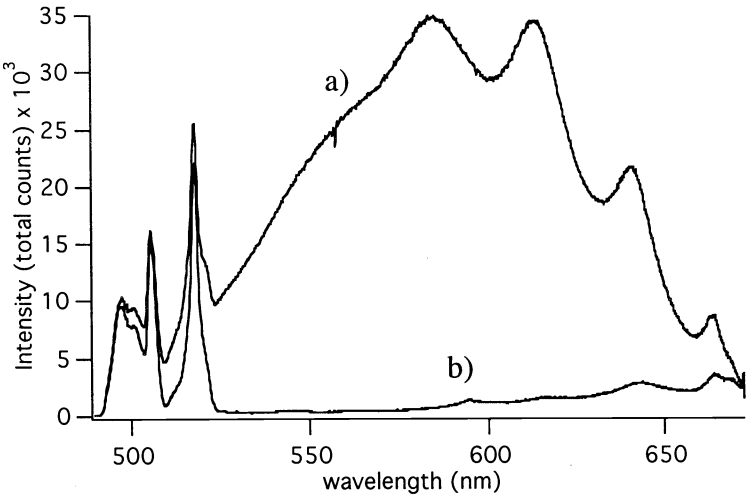

Fig. 4. Fluorescence spectra for for a) modified and b) unmodified IOG-1 glass.

Aside from the similarity in their atomic structure, the two defects have spectroscopic similarities. Both have similar absorption bands (POHC – 2.2, 2.5, 5.3 eV, NBOHC – 2.0, 4.8 eV) and fluorescence bands (NBOHC - 1.9 eV emission, POHC – 2.1 eV from our study). Furthermore, Sun *et al.* [22] have previously observed NBOHC formation in fused silica exposed to fs pulses that fluoresce at 650 nm.

3.3. Fluorescence imaging of modified glasses

Fluorescence imaging is performed to determine the spatial location of the color center defects within the modified glasses that are responsible for the fluorescence. In addition, since the defects are created directly by the fs laser pulses, fluorescence imaging also gives information about the regions in the material that are directly exposed to the laser beam. Figure 2-D1 shows the fluorescence image for the end face of a waveguide written in fused silica using ~ 1 μJ fs pulse energy with a 10x objective. From the fluorescence image, it is clear that the defects are created in the waveguide core regions. This indicates that the waveguide is created through direct exposure to the fs pulses.

Fluorescence imaging of the end face of the waveguides written in IOG-1 glass is also performed in the same manner. The results are shown in Figs. 2-D2 and 2-D3. The fluorescence images are nearly identical in both shape and dimension to the central, damage regions in the white light images. It is clear that, based on the comparison between the fluorescence and white light images, the color center defects responsible for the fluorescence are located primarily within the central, non-waveguiding, damage regions. No color center defects are formed in the waveguide regions surrounding the central region.

3.4. Photobleaching of color centers

In addition to the fluorescence at 600 nm and 630 nm that is observed when the modified glasses are illuminated with 488 nm light, we also observe that the fluorescence from both glasses decays with prolonged exposure to the excitation light. To accurately determine the decay behavior, an avalanche photodiode detector in the microscope setup is used to measure the total intensity of the fluorescence signal as a function of total continuous exposure time to the 488 nm excitation light. Figure 5 shows the fluorescence intensity as a function of time for different 488 nm powers used to probe a silica glass sample modified with 2 μJ of fs laser pulses. It is clear that the defects are being photobleached by the visible light and the decay process is dependent on the intensity of the probe beam.

For IOG-1 glass, the fluorescence also exhibits a decay response to continuous exposure to 488 nm light. More details about the photobleaching phenomena can be found in refs. 11 (fused silica) and 12 (IOG-1).

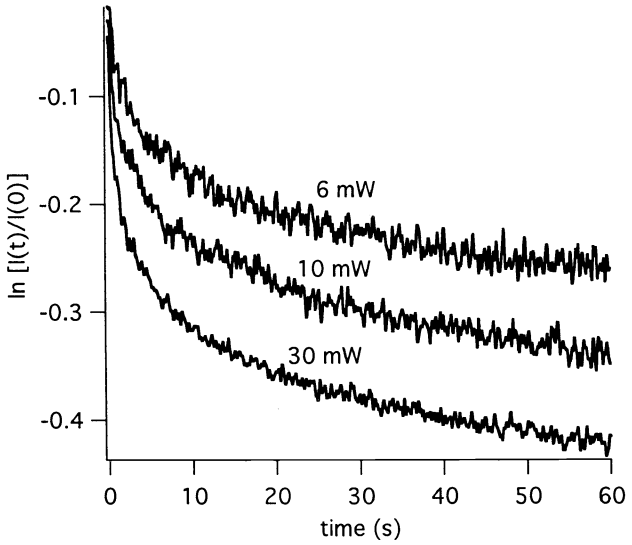

Fig. 5. Decay of 630 nm fluorescence from modified fused silica continuously exposed to different powers of 488 nm light.

3.5 Confocal Raman spectroscopy

In addition to the broad fluorescence bands in Figs 3 and 4 we also detect much lower intensity signals near 500 nm that are due to Raman scattering from the glass structural network. These signals sit on the edge of the broad fluorescence band. For analyzing the Raman signals, we subtract the fluorescence backgrounds from the overall spectra and normalize the Raman spectra. For fused silica the results have been described in detail in refs. 10 and 11. The most noticeable changes in the Raman spectra are increases in the intensity of two peaks at 490 and 605 cm^{-1} with increasing fs pulse energy. The 490 and 605 cm^{-1} Raman peaks are due to breathing modes from 4- and 3-membered ring structures in the silica network [23,24]. As discussed in refs. 10 and 11, the increase in the 490 and 605 cm^{-1} peak intensities corresponds to an increase in density and refractive index of the glass.

Raman spectroscopy is used to probe structural changes of fs-modified phosphate glass as well. As shown in Figs. 2 and 6, the modification in phosphate glasses leading to waveguide formation involves two distinct regions, a central damage region that does not function as a waveguide surrounded by regions that guide efficiently. The two different regions are each probed independently to determine the spectroscopic changes associated with each region. To accurately locate and probe each region, a fluorescence image of the end face (Fig. 6b)) is first obtained with the 488 nm light focused through a 100 X microscope objective. This image clearly defines the spatial location of the central non-guiding region (bright) and the waveguide regions that directly border this fluorescent region. The xyz translation stage is then moved to the proper coordinates so that each region is independently probed by the focused 488 nm beam for Raman signals. The Raman spectra for the unmodified glass and the central, non-waveguiding region are shown in Figure 6c. It should be noted that the Raman spectrum of the central, damage region initially is sitting on a 600 nm fluorescence background due to induced defects. The final spectrum is obtained by subtraction of the fluorescence background and normalization with respect to the 700 cm^{-1} peak. To interpret this data, it is necessary to understand the structural glass network of typical phosphate glasses. It is understood that the basic building blocks for phosphate glass are PO_4 tetrahedra. The tetrahedra link together through covalent bonding of the oxygen atoms. Depending on the concentration of modifier ions that break up, or depolymerize, the phosphate chains that are the basis of the glass network, the linked phosphate tetrahedra may have one, two, three, or all four of the oxygen atoms be non-bridging atoms. The vibrations of the various bonds in the phosphate glass network show up as several discrete peaks in the Raman spectrum. Several groups have previously characterized these Raman peaks. The broad peak in the low wavenumber region (below 600 cm^{-1}) is attributed to the internal network bending vibrations of the phosphate chains (both in chain PO_2 and OPO bending) [25-27]. The peak at

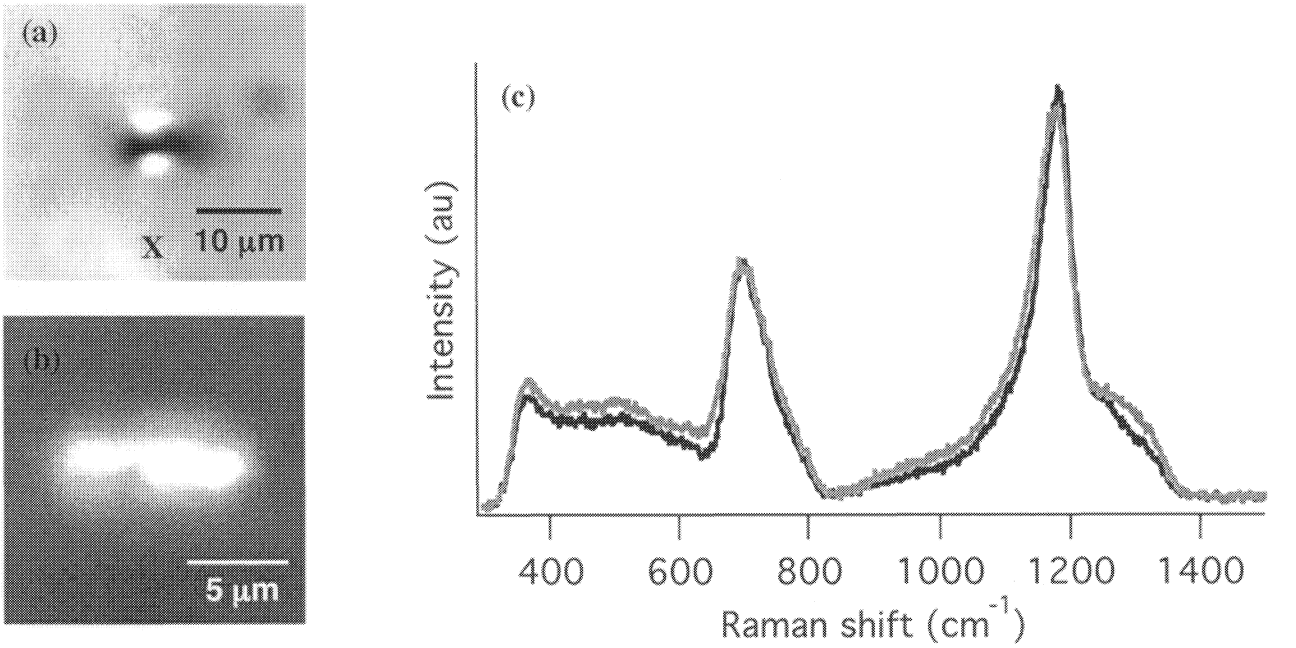

Fig. 6. (a) White light and (b) fluorescence image of the end view of fs laser-modified phosphate glass. (c) Raman spectra of initial (black) and fs-modified (red) phosphate glass. The red curve is obtained from the damaged, non-waveguiding region (marked with X in (a)).

700 cm^{-1} comes from the symmetric in-chain stretching vibration of an oxygen atom bridging two phosphate atoms [25,26,28,29]. The 1180 cm^{-1} peak is due to the PO_2 symmetric stretching, with the oxygens being non-bridging [25,28]. The 1260 cm^{-1} peak that sits on the shoulder of the 1180 cm^{-1} peak is the asymmetric stretching of the P-NBO bond [25,27,28].

The Raman changes observed in our study indicate that there are atomic scale structural changes in the glass network induced by fs pulses. The most noticeable change is an increase in the broad 1280 cm^{-1} peak. This peak, which lies on the shoulder of the 1180 cm^{-1} peak, has been previously assigned to the asymmetric stretching of non-bridging oxygen in O-P-O. This change may indicate that the energy deposited into the material by fs pulses breaks the phosphate chains in the glass network, resulting in the increase in the number of non-bridging oxygens attached to phosphorus atoms. The production of these phosphorus non-bridging oxygen hole centers in the modified glass is supported by the fluorescence at 600 nm observed in the modified material, which we have assigned to POHC defects. Other minor changes include a slight asymmetric broadening of the 1180 cm^{-1} peak, which is assigned to the symmetric stretching mode of the O-P-O and overall changes in the relative intensities of the Raman peaks. No noticeable Raman changes are observed when the two waveguide (non-fluorescent) regions are probed in the same manner. The absence of the Raman change in the non-fluorescent waveguiding region is also further evidence that the increase in the 1280 cm^{-1} peak involves breaking of bonds in the network leading to production of color center defects.

4. DISCUSSION

Our results show that the waveguides that we have fabricated using fs laser pulses, behave differently in fused silica and IOG-1 glass: in fused silica waveguides are formed in the focal region of the fs laser beam, whereas in IOG-1 they are formd in regions surrounding the exposed region.

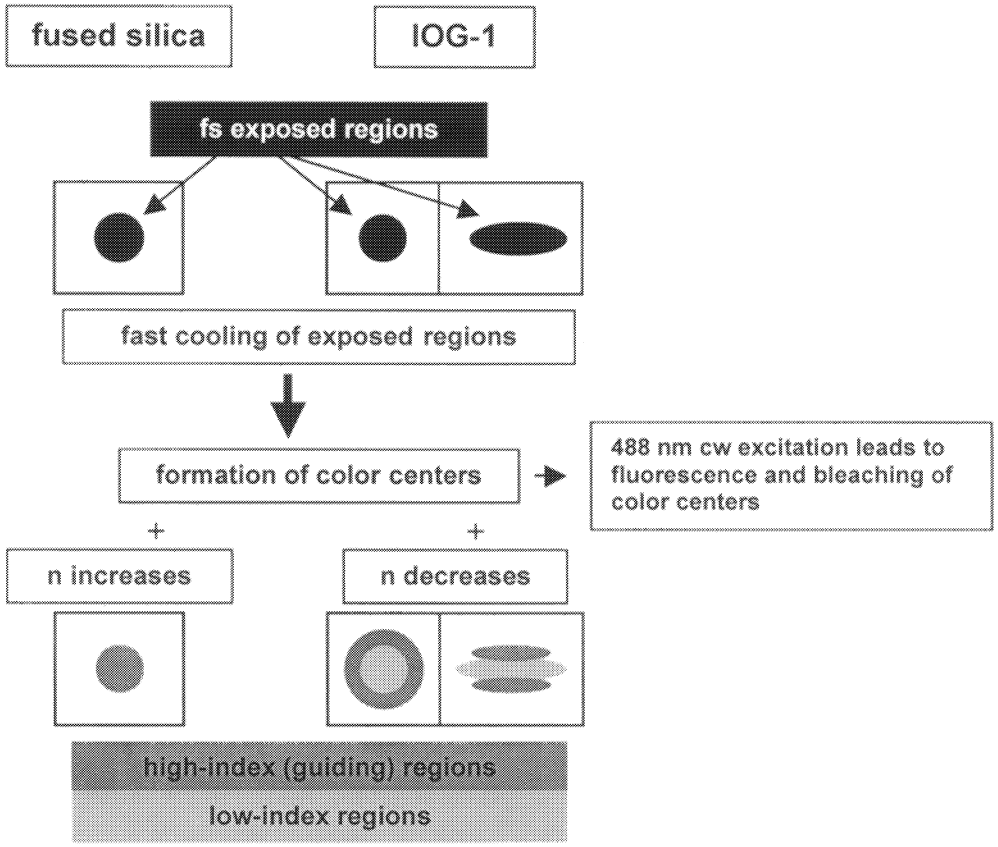

Fig. 7. Schematic diagram of the processes associated with fs-laser waveguide writing in fused silica and IOG-1 glass.

This difference in behavior can be understood by considering the processes that occur in the glass after the fs laser energy is deposited into the material. These processes are illustrated in fig. 7. In both glasses the fs laser energy is absorbed in the focal region and results in the formation of a localized hot plasma. Because the region that is exposed per pulse is very small (on the order of the focal volume) it will cool down/quench very fast before the arrival of the next pulse (1 ms later since the laser rep rate is 1 KHz). Therefore, the exposed region and resulting modified spot consists of glass with a much higher quenching rate and has a structure that is different from the original glass. This is confirmed by the fact that the modified spot shows fluorescence from NBOHC defects (resulting from bond-breaking) and a Raman spectrum that resembles a glass with high quench rates. Although the exposed region in both fused silica and IOG-1 has localized defects, the resulting change in refractive index is different. In fused silica the exposed region has a higher refractive index than the original glass, but in IOG-1 the index in the exposed region is lower. This is consistent with the dependence of the index on cooling rate. In fused silica the index increases with cooling rate [30] whereas in IOG-1 it decreases [13]. It should be pointed out that the lower index in the exposed region of IOG-1 is associated with an expansion of the structure and the waveguides that are observed above and below the exposed (central) region are the result of stress created by the expansion of the central region. The fact that color centers are not found in the waveguide regions of IOG-1, but only in the central region, lends supporting evidence that the waveguides are not created via direct exposure to the fs laser beam.

Finally we note that, although our results can be understood in terms of the dependence of the refractive index on cooling rate, we do not claim that the processes occurring in the exposed region are merely identical to those occurring during fast thermal quenching. It is well possible that other phenomena, such as shockwave propagation, are involved, especially at high fs pulse energies. For the relatively low fs pulse energies necessary to fabricate good waveguides the cooling rate model might be adequate and we are currently investigating how well this model describes fs-laser fabrication of waveguides in other glass systems.

ACKNOWLEDGEMENT

This work was performed under the auspices of the U.S. Department of Energy by the University of California, Lawrence Livermore National Laboratory, under contract No. W-7405-Eng-48. D. M. Krol acknowledges financial support through National Science Foundation grant ECS 0083087.

REFERENCES

1. K. M. Davis, K. Miura, N. Sugimoto and K. Hirao, Opt. Lett. **21**, 1729 (1996).
2. C. B. Schaffer, A. Brodeur, J. F. Garcia and E. Mazur, Opt. Lett. **26**, 93 (2001).
3. D. Homoelle, S. Wielandy, A. L. Gaeta, N. F. Borrelli and C. Smith, Opt. Lett. **24**, 1311 (1999).
4. Y. Sikorski, A. A. Said, P. Bado, R. Maynard, C. Florea and K. A. Winick, Electron. Lett. **36**, 226 (2000).
5. J. W. Chan, T. R. Huser, S. H. Risbud, D. M. Krol, Proceedings of SPIE Vol. **4640**, p129-236 (2002).
6. G. Cerullo, R. Osellame, S. Taccheo, M. Marangoni, D. Polli, R. Ramponi, P. Laporta, and S. De Silvestri, Opt. Lett. **27**, 1938 (2002).
7. T. Pertsch, U. Peschel F. Lederer, J. Burghoff, M. Will, S.Nolte and A. Tünnermann, Opt. Lett. **29**, 468 (2004).
8. A. Zoubir, M. Richardson, C. Rivero, A. Schulte, C. Lopez, K. Richardson Orlando, Florida N. Hô and R. Vallée, Opt. Lett. **29**, 748 (2004).
9. M. Will, S. Nolte and A. Tunnermann, Proc. SPIE **4633**, 99 (2002).
10. J. W. Chan, T. Huser, S. Risbud and D. M. Krol, Opt. Lett. **26**, 1726 (2001).
11. J.W. Chan T.R. Huser S.H. Risbud, D.M. Krol, Applied Physics A **76**, 367 (2003).
12. J. W.Chan, T. Huser, J. Hayden, S. Risbud and D. M. Krol, J. Am. Ceram. Soc. **85**, 1037 (2002).
13. J. W. Chan "Confocal Laser Spectroscopy of Glasses Modified by Ultrashort Laser Pulses for Waveguide Fabrication", Ph. D. Dissertation (University of California at Davis, Davis, CA, 2002).
14. J.W. Chan, T.R. Huser S.H. Risbud, J. S. Hayden, D.M. Krol, Appl. Phys. Lett. **82**, 2371 (2003).
15. L. Skuja, T. Suzuki and K. Tanimura, Phys. Rev. B **52** 15208 (1995).
16. L. Skuja, J. Non-Crystalline Solids **179** 51 (1994).
17. L. Skuja, K. Tanimura and N. Itoh, J. Appl. Phys. **80** 3518 (1996).

18. M. Cannas and M. Leone, J. Non-Crystalline Solids **280**, 183 (2001).
19. L. Skuja, M. Mizuguchi, H. Hosono and H. Kawazoe, Nucl. Instr. & Meth. Phys. Res. B **166** 711 (2000).
20. L. Skuja, M. Hirano and H. Hosono, Phys. Rev. Lett. **84**, 302 (2000).
21. M. Watanabe, S. Juodkazis, H. B. Sun, S. Matsuo and H. Misawa Phys. Rev. *B* **60** (14) 9959-9964 (1999).
22. H. B. Sun, S. Juodkazis, M. Watanabe, S. Matsuo, H. Misawa and J. Nishii, J. Phys Chem B **104** (15) 3450-3455 (2000).
23. F. L. Galeener, Journal of Non-Crystalline Solids **71,** 373 (1985).
24. A. Pasquarello and R. Car, Physical Review Letters **80** (23) 5145-5147 (1998).
25. S. H. Morgan, R. H. Magruder, III and E. Silberman J. Am. Ceram. Soc. **70** C378 (1987).
26. D. Ilieva, B. Jivov, G. Bogachev, C. Petkov, I. Penkov and Y. Dimitriev **283,** 195 (2001).
27. J. J. Hudgens, R. K. Brow, D. R. Tallant and S. W. Martin, J. Non-Crystalline Solids **223**, 21 (1998).
28. R. K. Brow and D. R. Tallant, J. Non-Crystalline Solids **222**, 396 (1997).
29. R. Lebullenger, L. A. O. Nunes and A. C. Hernandes, J. Non-Crystalline Solids **284**, 55 (2001).
30. R. Bruckner, J. Non-Cryst. Solids **5**, 123 (1970)